Catalysis Today 394-396 (2022) 314–324

Contents lists available at ScienceDirect

Catalysis Today

journal homepage: www.elsevier.com/locate/cattod

Simulation-based optimization of cycle timing for CO_2 capture and hydrogenation with dual function catalyst

Alejandro Bermejo-López, Beñat Pereda-Ayo, José A. González-Marcos, Juan R. González-Velasco *

Department of Chemical Engineering, Faculty of Science and Technology, Universidad del País Vasco UPV/EHU, Barrio Sarriena, s/n, 48940 Leioa, Bizkaia, Spain

ARTICLE INFO

Keywords:
Simulation
CO_2 hydrogenation
CO_2 storage
Methane production
Dual function material

ABSTRACT

CO_2 methanation could play a significant role in the future energy system. The excess of renewable electric energy can be transformed into storable methane to balance the energy demand when required. Moreover, the CO_2 methanation can be performed alternating steps of CO_2 storage and reduction, avoiding expensive CO_2 purification steps. In this work, we will use a previously developed and validated model to optimize by simulation the CO_2 adsorption and hydrogenation cycles timing (t_{CO2}/t_{H2}). The performance of the catalyst is quantified by the CO_2 conversion (X_{CO2}, %), H_2 conversion (X_{H2}, %) and CH_4 production (Y_{CH4}, mmol g^{-1} cycle^{-1}). Long adsorption and hydrogenation times result in high CH_4 productions per cycle, however, low CO_2 and H_2 conversion. Therefore, adsorption times close to the catalyst saturation (t_{CO2}=60 s) and moderate hydrogenation times are preferable. To better select the optimal hydrogenation time, a new catalytic parameter is set, the average formation rate of CH_4 ($\bar{r}_{CH_4}$, μmol g^{-1} s^{-1}). The optimal hydrogenation time is set at 120 s. In addition to having a high average formation rate of CH_4, t_{CO2}/t_{H2}= 60/120 cycle timing would allow to work with three identical beds in parallel, one in adsorption mode and two in regenerating mode. With the optimum cycle timing of 60/120 the production of CH_4 results in 148 μmol g^{-1} cycle^{-1} (1.2 μmol CH_4 g^{-1} s^{-1}) and a CO_2 and H_2 conversion of 25% and 43%, respectively

1. Introduction

The CO_2 methanation reaction (Eq. 1), also known as Sabatier reaction, originates in 1902 [1]. The scientific interest on the Sabatier's reaction has grown in recent years in the context of a massive implementation of renewable energies. One of the main drawbacks of renewable energies is their intermittent nature due to their dependence on atmospheric conditions. In an energy system based on renewable energies, periods of energy shortage or surplus can occur. Thus, the storage of energy to balance the energy demand is essential. In this context, the CO_2 methanation has a practical application. In periods of energy surplus, the electric energy produced by renewables energies would be used to produce hydrogen by electrolysis, which then reacts catalytically with CO_2 (captured from an industrial effluent) to produce CH_4 named as synthetic natural gas (SNG). This process is also known as Power to Gas (PtG) technology, which aims to connect the electric grid and the gas grid to make the future energy system more robust [2].

$$CO_2+4H_2 \leftrightarrows CH_4+2H_2O \quad (1)$$

Sabatier's reaction is characterized by being strongly exothermic, and therefore equilibrium is favored at low temperatures. On the other hand, the number of moles of products is less than that of reagents, so the thermodynamic equilibrium is favored at high pressures. However, working at high pressure implies a high economic cost, so it is more convenient to work at atmospheric pressure [3]. In addition, it should be noted that the complete reduction of CO_2 (oxidation state C^{+4}) to methane (oxidation state C^{-4}) implies the transfer of eight electrons, which implies to overcome a high kinetic barrier. Therefore, the use of catalysts is essential [4].

In general, the catalysts used for this reaction must have thermal stability in the operating temperature range of 200–400 °C. Catalysts with different active phases (Ru, Ni, Fe, Co.) [5–9], and different supports (Al_2O_3, zeolites, SiO_2, TiO_2.) [10–14] have been used in recent years. Among the active phases, nickel shows high CO_2 conversion and is one of the most used metals due to its abundance and low cost. However, nickel tends to sinter, and therefore, deactivate. On the other hand, ruthenium is very active, selective and stable towards methane formation even at low temperatures. Although Ru is more expensive than Ni, it

* Corresponding author.
E-mail address: juanra.gonzalezvelasco@ehu.eus (J.R. González-Velasco).

https://doi.org/10.1016/j.cattod.2021.08.023
Received 19 February 2021; Received in revised form 22 July 2021; Accepted 22 August 2021
Available online 26 August 2021

Nomenclature

C_i	Concentration of the component i (mmol cm^{-3})
D	Diffusion coefficient (cm^2 s^{-1})
E_i^0	Activation energy named i (J mmol^{-1})
F_i^{in}	Molar flow at the reactor inlet of the component i (mmol min^{-1})
F_i^{out}	Molar flow at the reactor outlet of the component i (mmol min^{-1})
k_i	Kinetics constant number i (see reference [26])
k_i^0	Preexponential factor number i (J mmol^{-1})
K_{eq}	CO_2 hydrogenation equilibrium constant (atm^{-2})
m	Adjust parameter (dimensionless)
r_i	Reaction rate of the component i (mmol g^{-1} s^{-1})
$\bar{r}_{CH_4}$	Average formation rate of CH_4 (mmol g^{-1} s^{-1})
R	Ideal gas constant (J K^{-1} mmol^{-1})
t	Time (s)
t_{CO2}	Time of the storage step (s)
t_{H2}	Time of the hydrogenation step (s)
T	Temperature (K)
x	Axial position (cm)
X_{CO2}	CO_2 conversion (%)
X_{H2}	H_2 conversion (%)
Y_{CH4}	CH_4 production (μmol g^{-1})

Greek symbols

α	Correction factor (dimensionless)
ε	Porosity (dimensionless)
θ_i	Covering factor of the component i (dimensionless)
ρ	Density (g cm^{-3})
Ω	Adsorption capacity (mmol g^{-1})
Ω_{max}	Maximum adsorption capacity (mmol g^{-1})

Acronyms

DFM	Dual Function Material
PDE	Partial Differential Equation
SNG	Synthetic Natural Gas

has been reported in a large number of publications [9,15]. On the other hand, the support can influence the dispersion of the active phases, its reducibility and the formation of spinels that can reduce the activity of the catalyst [16]. Generally, basic mesoporous solids are used; in particular, alumina has been the most used support to disperse the active phase.

In the early 2020 there were 38 methanation plants with a total capacity of 14.5 MW and that number is growing exponentially [17]. One of the main drawbacks of PtG technology is the high costs associated with the CO_2 purification. One cost effective alternative is the utilization of a dual-function material (DFM) as catalyst. The DFM contains an alkaline or alkaline earth element that acts as an adsorbent and a noble metal that assists the methanation reaction [18,19]. The DFM allows the capture of CO_2 and its direct conversion to methane, without the need of intermediate CO_2 sequestration processes, which are energy intensive. The operation is carried out cyclically alternating steps of CO_2 storage and hydrogenation. This novel operative strategy has recently been proposed by Duyar et al. [20]. CO_2 is first captured onto the basic element of the catalyst until saturation. Afterwards, H_2 is injected and favors a spillover phenomenon that conducts the chemisorbed CO_2 to the metal site where the methanation takes place. Both the CO_2 capture process and the CH_4 production process can operate at a temperature of 250–400 °C. An effluent of a combustion process can easily reach this temperature. Thus, the PtG technology using DFMs can be directly applied, without the need for an external heat input [21,22].

This novel cyclic operation strategy is very promising. However, it still needs further development for industrial implementation. Advances in the formulation and physyco-chemical properties of DFMs are required to boost the adsorption capacity and hydrogenation activity of the samples. In this sense, an intimate contact between the adsorbent and the metal is crucial [22]. On the other hand, the influence of the operational variables on the CO_2 adsorption and hydrogenation performance has to be addressed. This experimental work is usually a very time consuming step if the number of studied variables is so large to cover a wide range study. One possibility to predict the influence of operational variables on the catalytic behavior is simulation. For that, it is required to build first a robust model able to predict accurately the evolution of reactants and products under a wide range of operational conditions.

In own previous work [23–25], we reported a complete reaction scheme able to describe the CO_2 adsorption and hydrogenation using DFMs with formulation x-Na_2CO_3/Al_2O_3 (x = Ru/Ni). Briefly, CO_2 and H_2O compete for the adsorption sites (Na_2O), forming the corresponding carbonate (Na_2CO_3) or hydroxide (NaOH), respectively. During the adsorption step, a CO_2 molecule can displace a previously adsorbed H_2O molecule, forming the carbonate and releasing H_2O to the gas phase. During the hydrogenation step, the as-formed carbonates are decomposed and hydrogenated on the metal site producing CH_4 and H_2O. Some fraction of the as-formed H_2O is adsorbed onto the storage sites forming the hydroxide.

Based on the elemental reactions that govern the process, we proposed a kinetic model, which accurately predicts the evolution of CO_2, CH_4 and H_2O [26]. The kinetic equations of the model rely on the concentration of reactants and products and on the surface coverage of CO_2 and H_2O. The model was validated in a wide range of reactants concentrations, i.e. 1.4–10.9% CO_2 during the adsorption step and 1.4–10.9% H_2 during the hydrogenation step, and in the 250–400 °C temperature range.

In this work, we shall use the previously developed and validated model to optimize by simulation modeling the duration of the CO_2 storage step and the duration of the hydrogenation step, i.e. the CO_2 adsorption and hydrogenation cycles timing (t_{CO2}/t_{H2}). First, different simulations are performed with different t_{CO2}/t_{H2} to qualitatively observe how the pair of times influences on the temporal evolution of CO_2, CH_4 and H_2O. The surface coverages of CO_2 and H_2O are also analyzed at this point. Then, catalytic parameters are defined with which the global performance of the catalyst can be evaluated at any given t_{CO2}/t_{H2}. The conversion of CO_2 and H_2, CH_4 yield and the average CH_4 formation rate are analyzed in order to define an optimum CO_2 adsorption and hydrogenation cycle timing (t_{CO2}/t_{H2}). Based on the optimal cycle timing, a reactor configuration is proposed for the industrial application.

2. Experimental

2.1. Catalyst preparation and reaction test procedure

A dual function material with formulation 4%Ru-10%Na_2CO_3/Al_2O_3 was prepared by wet impregnation. A detailed description of the preparation procedure and characterization of the catalyst can be found elsewhere [26]. Reactor tests were performed in a stainless steel tube placed in a vertical furnace. 3 g of pelletized (0.3–0.5 mm) catalyst was housed in the reactor. The catalyst was pre-treated with a gas stream composed of 10% H_2/Ar at 350 °C for 45 min to favor the reduction of Ru.

The CO_2 storage and hydrogenation is carried out with cyclic feeding. During the CO_2 storage step, a gas stream composed of 5.7% CO_2/Ar was fed for 2.5 min. During the hydrogenation step, a gas stream composed of 5.7% H_2/Ar was fed for 5 min. A purging step with argon was fed between adsorption and hydrogenation cycles to avoid mixing of both gas streams. The operation was carried out at 350 °C and the total flowrate was set at 1200 ml min^{-1}, which corresponds to a space velocity of 15,000 h^{-1}. The composition of the gas stream leaving the reactor was analyzed by FTIR (MKS MultiGas 2030) for quantitative determination of CO_2, CH_4 and H_2O concentration.

The CO_2 adsorption capacity (Ω) during the storage period is calculated by Eq. (2). CH_4 and H_2O productions are calculated by Eqs. (3) and (4), respectively.

$$\Omega\left(\text{mmol g}^{-1}\right) = \frac{1}{W}\int_0^{t_{CO_2}}\left[F_{CO_2}^{in}(t) - F_{CO_2}^{out}(t)\right]dt \quad (2)$$

$$Y_{CH_4}\left(\text{mmol g}^{-1}\right) = \frac{1}{W}\int_0^{t_{H_2}} F_{CH_4}^{out}(t)dt \quad (3)$$

$$Y_{H_2O}\left(\text{mmol g}^{-1}\right) = \frac{1}{W}\int_0^{t_{H_2}} F_{H_2O}^{out}(t)dt \quad (4)$$

t_{CO2} and t_{H2} correspond to the duration of the CO_2 storage and hydrogenation periods, respectively. $F_{CO_2}^{in}$ and $F_{CO_2}^{out}$ correspond to the CO_2 molar flow at the reactor inlet and outlet streams, respectively. $F_{CH_4}^{out}$ and $F_{H_2O}^{out}$ are the molar flows of CH_4 and H_2O at the reactor outlet stream, respectively. W is the weight of the catalyst housed in the reactor.

Two additional parameters will be used to evaluate the catalytic performance, i.e. the conversion of CO_2 and the conversion of H_2 during the hydrogenation period.

$$X_{CO_2} = \frac{\int_0^{t_{CO_2}}\left[F_{CO_2}^{in}(t) - F_{CO_2}^{out}(t)\right]dt}{\int_0^{t_{CO_2}} F_{CO_2}^{in}(t)dt}\cdot 100 = \frac{\int_0^{t_{H_2}} F_{CH_4}^{out}(t)dt}{\int_0^{t_{CO_2}} F_{CO_2}^{in}(t)dt}\cdot 100 \quad (5)$$

$$X_{H_2} = \frac{\int_0^{t_{H_2}}\left[F_{H_2}^{in}(t) - F_{H_2}^{out}(t)\right]dt}{\int_0^{t_{H_2}} F_{H_2}^{in}(t)dt}\cdot 100 = \frac{4\int_0^{t_{H_2}} F_{CH_4}^{out}(t)dt}{\int_0^{t_{H_2}} F_{H_2}^{in}(t)dt}\cdot 100 \quad (6)$$

All the CO_2 stored reacts to form CH_4, i.e. unreacted CO_2 is not experimentally observed during the hydrogenation period, as will be seen later. Thus, the amount of CO_2 stored can be also evaluated as the amount of CH_4 produced during the hydrogenation step: $\int_0^{t_{H_2}}[F_{CO_2}^{in}(t) - F_{CO_2}^{out}(t)]dt = \int_0^{t_{H_2}} F_{CH_4}^{out}(t)dt$, provided that Sabatier's reaction stoichiometry states 1 mol CO_2:1 mol CH_4. On the other hand, H_2 conversion can be calculated based on methane formation. For that, it is considered that hydrogen consumption quadruples methane formation, following again the stoichiometry of the Sabatier's reaction (Eq. 1).

2.2. Reactor model

Dynamic one dimensional isothermal heterogeneous plug flow reactor model with axial dispersion is considered for the modeling of the CO_2 capture and hydrogenation. The evolution of the concentration of CO_2, CH_4 and H_2O is calculated by solving jointly the partial differential equation (PDE) for the gas phase (Eq. 7) and the ordinary differential equation (ODE) for the solid phase (Eq. 8).

$$\text{Gas phase}: \frac{\partial C_i}{\partial t} = -\frac{u}{\varepsilon}\frac{\partial C_i}{\partial x} + \frac{D}{\varepsilon}\frac{\partial^2 C_i}{\partial x^2} + \frac{\rho r_i}{\varepsilon} \quad (7)$$

$$\text{Adsorbent phase}: \frac{\partial \theta_j}{\partial t} = \frac{R_i}{\Omega_{max}} \quad (8)$$

where ε is the void fraction, C_i the concentration of the gas phase of species i, θ_j is the surface coverage of species j, u the linear velocity of the gas, D the diffusion coefficient, ρ the density of the bed, x the axial coordinate of the reactor, Ω_{max} the maximum CO_2 adsorption capacity of the catalyst, and R_i the rate of formation of species i, calculated according to:

$$R_i = \sum_{k=1} r_k \upsilon_{i,k} \quad (9)$$

where i is the index of the species considered, r_k the intrinsic velocity of reaction k and $\nu_{i,k}$ the stoichiometric coefficient of species i in reaction k.

We reported in a previous work [24] the mechanism of the CO_2 storage and hydrogenation to CH_4 using a dual function material that operates in alternate cycles. The main reactions occurring during adsorption period are:

$$Na_2O + CO_2 \leftrightarrows Na_2CO_3 \quad (10)$$

$$2NaOH + CO_2 \leftrightarrows Na_2CO_3 + H_2O \quad (11)$$

$$NaOH + CO_2 \leftrightarrows NaHCO_3 \quad (12)$$

and during methanation period:

$$Na_2CO_3 \leftrightarrows Na_2O + CO_2 \quad (13)$$

$$CO_2 + 4H_2 \leftrightarrows CH_4 + 2H_2O \quad (1)$$

$$Na_2O + H_2O \leftrightarrows 2NaOH \quad (14)$$

Check out reference [24] for more details regarding the CO_2 adsorption and hydrogenation mechanism. The kinetic equations used by the model are based on those reactions. A detailed discussion about the kinetic expressions adopted by the model can be also found in our previous work [26]. The kinetic expressions used to predict the reaction rates of CO_2, CH_4 and H_2O during the adsorption, purge and hydrogenation period are collected in Table 1.

The temporal evolution of the concentration of CO_2, CH_4 and H_2O predicted by the model was obtained by integrating the mass balance for the gas phase (Eq. 7) and for the solid phase (Eq. 8). The model considers that CO_2 and H_2O can be adsorbed onto the storage sites (Na_2O) leading to the formation of carbonates (Na_2CO_3) and hydroxides (NaOH). The presence of carbonates and hydroxides in the surface of catalysts containing a basic element, such as Na_2O or CaO, has been confirmed by FTIR when exposed to gas phase CO_2 or H_2O [27]. The kinetic expressions adopted in the model for the estimation of the reaction rates rely on the surface coverage of CO_2 (θ_{CO2}) and H_2O (θ_{H2O}). The surface coverage of CO_2 is defined as the amount of CO_2 adsorbed in the storage sites (Ω) with respect to the maximum CO_2 storage capacity (Ω_{max}). Thus, if the catalyst is saturated with CO_2, the surface coverage of CO_2 would be 1 (θ_{CO2}=1). On the contrary, if the catalyst is fully regenerated, the surface coverage of CO_2 would be 0 (θ_{CO2}=0). Depending on the state of the catalyst, the covering factor takes values comprised between $0 \leq \theta_{CO2} \leq 1$. The surface coverage of H_2O is defined as the amount of H_2O adsorbed in the storage sites with respect to the maximum CO_2 storage capacity (Ω_{max}). As observed for θ_{CO2}, depending on the state of the catalyst, the covering factor of H_2O takes values comprised between $0 \leq \theta_{H2O} \leq 1$. Taking into account the adsorption stoichiometry of CO_2 and H_2O (Eq. 10 and Eq. 14) one molecule of CO_2 or one molecule of H_2O is adsorbed onto one molecule of the storage site (Na_2O). As CO_2 and H_2O compete for the same adsorption sites, at any time $0 \leq \theta_{CO2} + \theta_{H2O} \leq 1$. Besides, the model also considers the formation of bicarbonate type species (Eq. 12) when CO_2 and H_2O coexist in the gas phase. Note that formation of bicarbonates means that one additional molecule of CO_2 and H_2O are adsorbed onto and already carbonated adsorption site (Na_2CO_3). A global reaction scheme for bicarbonates formation was proposed in our previous work [26], in which CO_2 is delivered by a neighborhood adsorption site and H_2O is adsorbed from the gas phase. Thus, the formation of bicarbonates is considered as an unstable reservoir for the storage of H_2O without implication in the storage of CO_2. The surface coverage of bicarbonates is defined as $\theta_{H2O/CO2}$. In the presence of bicarbonates, the sum of the surface coverages of CO_2 (θ_{CO2}),

Table 1
Kinetic expressions used to predict the reaction rates of CO_2, CH_4 and H_2O during the adsorption, purge and hydrogenation periods.

CO_2 adsorption	Eq.
$(r_{CO_2})_{storage} = -k_1 C_{CO_2}(1-\theta_{CO_2}-\theta_{H_2O}) - k_2 C_{CO_2}\theta_{H_2O}$	(15)
$(r_{CH_4})_{storage} = 0$	(16)
$(r_{H_2O})_{storage} = k_2 C_{CO_2}\theta_{H_2O} - k_3 C_{H_2O}(1-\theta_{CO_2}-\theta_{H_2O}) - k_4\frac{C_{H_2O}\theta_{CO_2}}{1+K_{CO_2}C_{CO_2}^m} + k_5 C_{CO_2}\theta_{H_2O/CO_2}$	(17)
Purge	Eq.
$(r_{CO_2})_{purge} = k_6^0 \exp\left[-\frac{E_6^0}{RT}(1-\alpha\theta_{CO_2})\right]\theta_{CO_2}$	(18)
$(r_{CH_4})_{purge} = 0$	(19)
$(r_{H_2O})_{purge} = k_2 C_{CO_2}\theta_{H_2O} - k_3 C_{H_2O}(1-\theta_{CO_2}-\theta_{H_2O}) - k_4\frac{C_{H_2O}\theta_{CO_2}}{1+K_{CO_2}C_{CO_2}^m} + k_5 C_{CO_2}\theta_{H_2O/CO_2}$	(20)
Hydrogenation	Eq.
$(r_{CO_2})_{hydrogenation} = k_7^0 \exp\left(-\frac{E_7^0}{RT}\right)\theta_{CO_2}C_{H_2} - (r_{CH_4})_{hydrogenation}$	(21)
$(r_{CH_4})_{hydrogenation} = k_8^0 \exp\left(-\frac{E_8^0}{RT}\right)\left(P_{CO_2}^n P_{H_2}^{4n} - \frac{P_{CH_4}^n P_{H_2O}^{2n}}{[K_{eq}(T)]^n}\right)$	(22)
$(r_{H_2O})_{hydrogenation} = 2(r_{CH_4})_{hydrogenation} - k_{10}^0 \exp\left(-\frac{E_{10}^0}{RT}\right)C_{H_2O}(1-\theta_{CO_2}-\theta_{H_2O}) + k_9\theta_{H_2O}$	(23)

H_2O (θ_{H2O}) and ($\theta_{H2O/CO2}$) could exceed 1, as a H_2O molecule is adsorbed onto an already carbonated site.

As defined in the previous paragraph, the surface coverages of CO_2 (θ_{CO2}), H_2O (θ_{H2O}) and ($\theta_{H2O/CO2}$) are all defined as the amount of adsorbed specie divided by the maximum CO_2 storage capacity (Ω_{max}). In order to experimentally calculate $\Omega_{max,}$ CO_2 adsorption and hydrogenation cycles are carried out provided that the regeneration period is extended until complete regeneration of the catalyst. We consider full regeneration of the catalyst when carbon containing products (CH_4) are not observed at the reactor outlet stream, i.e. concentration is below 5 ppm. The subsequent CO_2 adsorption period is extended until the catalyst is saturated with CO_2. Under this experimental conditions, i.e. full regeneration during the hydrogenation period and full saturation during the adsorption period, the maximum CO_2 storage capacity (Ω_{max}) is calculated by Eq. (2).

Due to the cyclic nature of the operation, which alternates among different feeding compositions during the adsorption or hydrogenation periods, it is important to model how the feed enters the reactor. We showed in our previous work [26], that a first order transfer function was able to describe the evolution of CO_2 concentration at the reactor entrance when the CO_2 concentration is changed in step mode from 0% to 5.7% and from 5.7% to 0%. A first order transfer function was also applied to model the feeding of hydrogen at the beginning and at the end of the hydrogenation period.

To solve the PDE system, the axial coordinate of the reactor was discretized based on finite differences in 19 equidistant elements. Backward and central differences were applied for the evaluation of the first and second derivatives of the concentration with respect to the reactor length, respectively. To solve the system of resulting ordinary differential equations, a program was developed in *Matlab*.

The model has already been validated in our previous work [26] in a wide range of reactants concentration and temperature. Even though, as an example, Fig. S1 shows the temporal evolution of experimental gas phase CO_2, H_2O and CH_4 concentration together with that simulated by the model. The operation is carried out at 350 °C feeding a gas stream composed of 5.7% CO_2/Ar during the storage period and 5.7% H_2/Ar during the hydrogenation period. The duration of the storage period is 2.5 min and an Ar purge is continued for 2 min. Then the hydrogenation period is extended for 5 min and finally another Ar purge is performed for 1 min before starting a new cycle. As can be observed, the model accurately predicts the experimental evolution of gas phase CO_2, H_2O and CH_4 during the CO_2 adsorption and hydrogenation. Besides, the evolution of the covering factors at the reactor exist are also shown.

The kinetic parameters that best fit the experimental data were calculated based on the least squares method, using the concentrations of gaseous species (CO_2, CH_4 and H_2O) as experimental responses and the values are collected in the Table S1.

3. Results

3.1. Mechanism and kinetic modeling of the CO_2 adsorption and hydrogenation

Fig. 1 shows the temporal evolution of gas phase CO_2, CH_4 and H_2O predicted by the model when the operation is carried out at 350 °C. A gas stream composed of 5.7% CO_2/Ar is fed to the reactor during the CO_2 adsorption period, which is extended for 80 s. After the purging period with Ar for 120 s, a gas stream composed of 5.7% H_2/Ar is fed to the reactor. The hydrogenation period is extended for 160 s. The

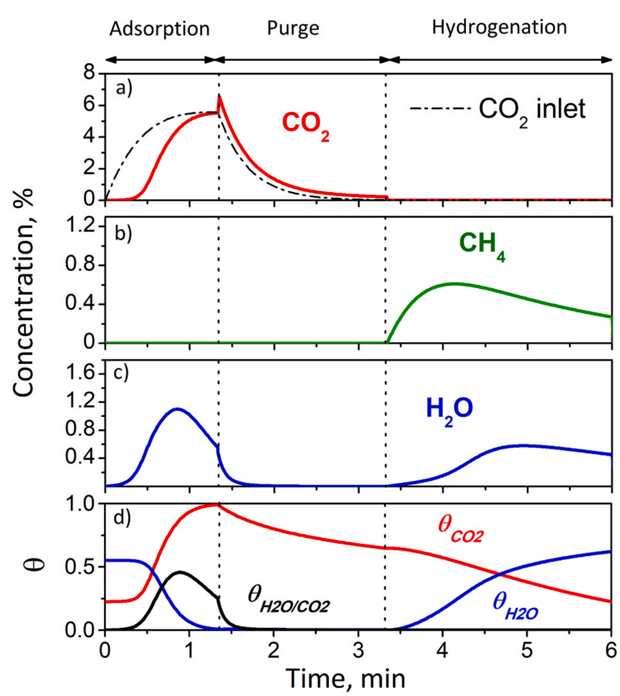

Fig. 1. Simulated CO_2, CH_4 and H_2O concentration profiles, together with the covering factors at the reactor exit, during one CO_2 adsorption and hydrogenation cycle with $4Ru10Na_2CO_3/Al_2O_3$ DFM. The CO_2 inlet profile (thin black line chart a) is also included. The temperature is fixed at 350 °C and the adsorption and hydrogenation period times in 80 and 160 s, respectively.

covering factors for the last axial coordinate (in which the reactor has been discretized for the integration of the system of ODEs) are also collected in Fig. 1d. The dynamics of the CO_2 capture and hydrogenation can be explained based on the main reactions that govern the process [23,24].

During the adsorption period, CO_2 is stored onto the basic sites of the catalyst (Na_2O) in the form of carbonates (Na_2CO_3) through Eq. (10). Alternatively, CO_2 can be also stored onto the hydrated form of the adsorption sites (NaOH) to form the carbonate through Eq. (11). Note that this route implies the release of H_2O to the gas phase, i.e. CO_2 displaces adsorbed H_2O to form the carbonate. Eqs. (10) and (11) are the main reactions describing the CO_2 storage process. The CO_2 storage onto the catalyst can be evidenced by comparing the CO_2 concentration signal at the reactor inlet (dotted line in Fig. 1a) and outlet streams (red line). Note that the CO_2 concentration is lower at the reactor outlet with respect to that observed in the inlet stream, which highlights the CO_2 adsorption capacity of the catalyst. In fact, the area comprised between the CO_2 concentration signal at the reactor inlet and outlet streams can be directly related with the CO_2 storage capacity of the catalyst. See Fig. S2 in supplementary material for detailed mathematical procedure to calculate the CO_2 storage capacity of the catalyst.

At the beginning of the CO_2 storage period, the adsorption of CO_2 occurs through Eq. (10). Afterwards, once the sodium oxide (Na_2O) sites have been completely carbonated, the storage of CO_2 can proceed through Eq. (11). Following the reaction stoichiometry, one molecule of H_2O is released to the gas phase when one molecule of CO_2 is stored. Thus, the storage of CO_2 through Eq. (11) can be evidenced by the presence of gas phase H_2O. As can be observed in Fig. 1c, water concentration breakthrough is detected after 0.25 min (15 s) of the storage period. Thus, for storage times lower than 15 s, the storage of CO_2 proceeds through Eq. (10) (without the release of H_2O), and afterwards through Eq. (11), as evidenced by the increase of the H_2O concentration. As the storage period proceeds, the covering factor of CO_2 (θ_{CO2}) increases and the covering factor of H_2O (θ_{H2O}) decreases, as can be observed in Fig. 1d. Eventually, all the storage sites of the catalyst become carbonated. Hence, the concentration of CO_2 at the reactor outlet matches that of the inlet (Fig. 1a) and the CO_2 covering factor reaches the value of 1 (Fig. 1d). When the catalyst is saturated with CO_2 no additional H_2O is released to the gas phase and the concentration of H_2O progressively decreases (Fig. 1c). When H_2O and CO_2 coexist in the gas phase, formation of bicarbonates is possible through Eq. (12). Indeed, bicarbonates covering factor ($\theta_{CO2/H2O}$) describes a maximum and then decreases following the decreasing trend observed for H_2O concentration. The evolution of CO_2 and H_2O concentration during the storage period is governed by the kinetic equations of the model.

After the storage period, CO_2 is removed from the feed stream and the catalyst is purged with Ar for two minutes, observing that the CO_2 concentration decreases progressively to practically zero. A slight decrease in θ_{CO2} is observed (Fig. 1d), due to the desorption of part of CO_2 that is weakly adsorbed. This process has been described by Eq. (13) and is modeled by Eq. (18) using a Temkin-type desorption kinetics. At the beginning of the purging period, the covering factor of water (θ_{H2O}) is zero because water has been completely displaced from the adsorption sites due to CO_2 adsorption. Meanwhile, bicarbonates decomposition is accelerated by the elimination of gas phase CO_2, which reduces their stability. Thus, the covering factor of bicarbonates ($\theta_{CO2/H2O}$, Fig. 1d) is rapidly reduced to zero. The H_2O formation rate during the CO_2 storage period is also valid for the purging period (Eq. 20).

Finally, the hydrogenation period begins admitting 5.7% H_2 in the feed. The inclusion of hydrogen provokes the decomposition of adsorbed CO_2, which is represented by Eq. (13) and is modeled by the first term of Eq. (21). This reaction pathway can be facilitated by the lower stability of carbonates in the presence of H_2 or by a catalytic process involving the spillover of hydrogen ad-atoms to the adsorption sites [28]. In the presence of gas phase CO_2 and H_2, the Sabatieŕs reaction (Eq. 1) proceeds and CH_4 and H_2O are produced. Thus, just from the beginning of the hydrogenation period CH_4 formation is detected. The formation of CH_4 is modeled with a potential kinetic equation recently reported by Falbo et al. [29] (Eq. 22). Note that during the whole hydrogenation period, gas phase CO_2 is not observed, which highlights that the CO_2 methanation rate (r_{CH4}) is higher than the CO_2 decomposition rate (expressed by the first term of Eq. 21). As the hydrogenation period proceeds, CH_4 formation is observed while the covering factor of CO_2 (θ_{CO2}, Fig. 1d) decreases progressively. The progressive diminution of the CO_2 covering factor indicates that the adsorption sites of the catalyst are being regenerated. Due to the progressive reduction of the CO_2 covering factor, the carbon source to be hydrogenated is reduced, and consequently, CH_4 formation progressively decreases in the last section of the hydrogenation period.

Water formation is also observed at the outlet of the reactor during the hydrogenation period (Fig. 1c). According to the Sabatieŕs reaction (Eq. 1), water formation should double CH_4, and should present a similar concentration profile. However, this is not observed in Fig. 1. The reason is that water interacts with the adsorption sites and is adsorbed, as described by Eq. (14). The consequence is that water formation in the gas phase is retarded with respect to CH_4. Due to water adsorption on the storage sites, the covering factor of water (θ_{H2O}) increases progressively during the hydrogenation period. Water formation during the hydrogenation period is modeled by Eq. (23).

3.2. *Dynamics of dual operation as a function of CO_2 adsorption and hydrogenation periods timing*

Up to now, the mechanism of the CO_2 storage and hydrogenation has been presented together with the kinetic equations used to model the operation. Now, we will focus on the influence of the adsorption and hydrogenation periods timing on the dynamics of the dual operation. For that, we will use the temporal evolution of the concentration of CO_2, H_2, CH_4 and H_2O as predicted by the model.

Fig. 2 shows the evolution of reagents and products concentration, together with the covering factors, for different adsorption and hydrogenation periods timing, i.e. t_{CO2} and t_{H2}, respectively. The concentration of CO_2 and H_2 at reactor inlet (dotted line) is also displayed in the corresponding charts. We have selected three scenarios to understand the influence of the adsorption and hydrogenation periods timing. In Fig. 2a we have selected t_{CO2}= 45 s and t_{H2}= 300 s as representative of a short adsorption period and long hydrogenation period. In Fig. 2b we have selected t_{CO2}= 150 s and t_{H2}= 300 s as representative of long adsorption and hydrogenation periods. Finally, in Fig. 2c we have selected t_{CO2}= 150 s and t_{H2}= 60 s as representative of long adsorption period and short hydrogenation period. Depending on the adsorption and hydrogenation periods timing, large differences are observed in the evolution of gas phase CO_2, H_2, CH_4 and H_2O concentrations, which we will explain in detail below. Note that the evaluation of the CO_2 adsorption and hydrogenation performance has to be done in the whole operation, considering the adsorption and hydrogenation performances. As this is a cyclic operation, alternating consecutive adsorption and hydrogenation periods, the state of the catalyst at the beginning of a given period depends on the state of the catalyst at the end of the previous period. For example, the CO_2 adsorption performance will be dependent on the state of the catalyst at the end the previous hydrogenation period. The same is applied for the hydrogenation period, which performance also depends on the state of the catalyst at the end of the previous adsorption period.

3.2.1. *Short adsorption period and long hydrogenation period scenario (t_{CO2}/t_{H2}=45/300)*

As can be observed in the upper chart of Fig. 2a, an adsorption period of 45 s does not achieve the saturation of the catalyst with CO_2. Note that at the end of the adsorption period, the CO_2 concentration at the reactor outlet is notably below the CO_2 concentration at the reactor inlet. Besides, the CO_2 covering factor depicted in the lower chart shows

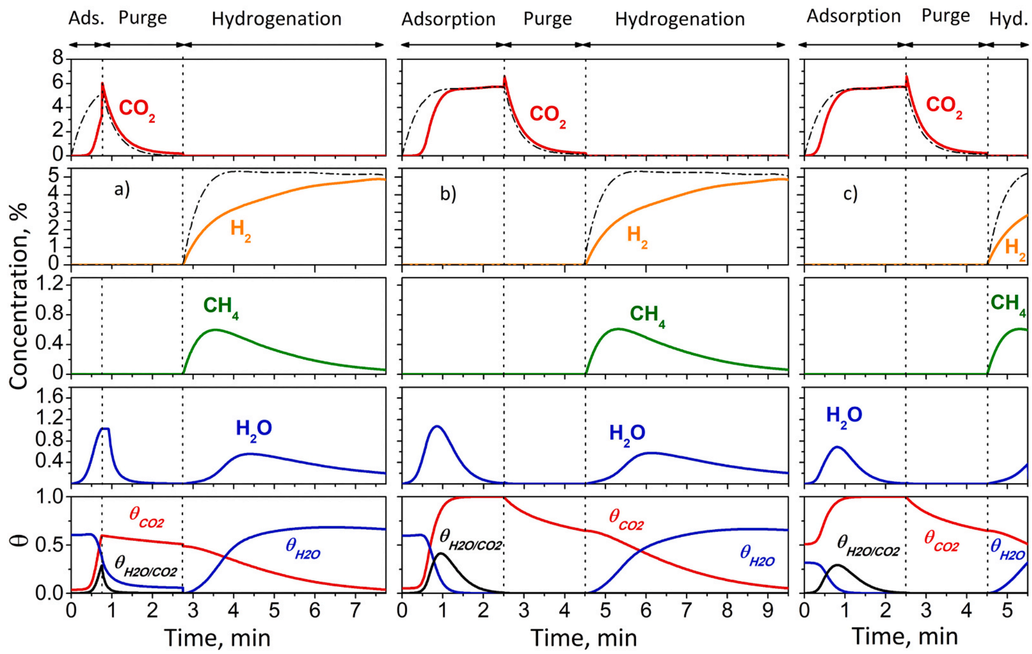

Fig. 2. Simulated CO_2, H_2, CH_4 and H_2O concentration profiles, together with the covering factors at the reactor exit, during one CO_2 adsorption and hydrogenation cycle with $4Ru10Na_2CO_3/Al_2O_3$ DFM. The CO_2 and H_2 inlet profiles (thin black lines charts a and b) is also included. The temperature is fixed at 350 °C and the adsorption and hydrogenation period times in t_{CO2}/t_{H2}= 45/300 (scenario a), t_{CO2}/t_{H2}= 150/300 (scenario b) and t_{CO2}/t_{H2}= 150/60 (scenario c).

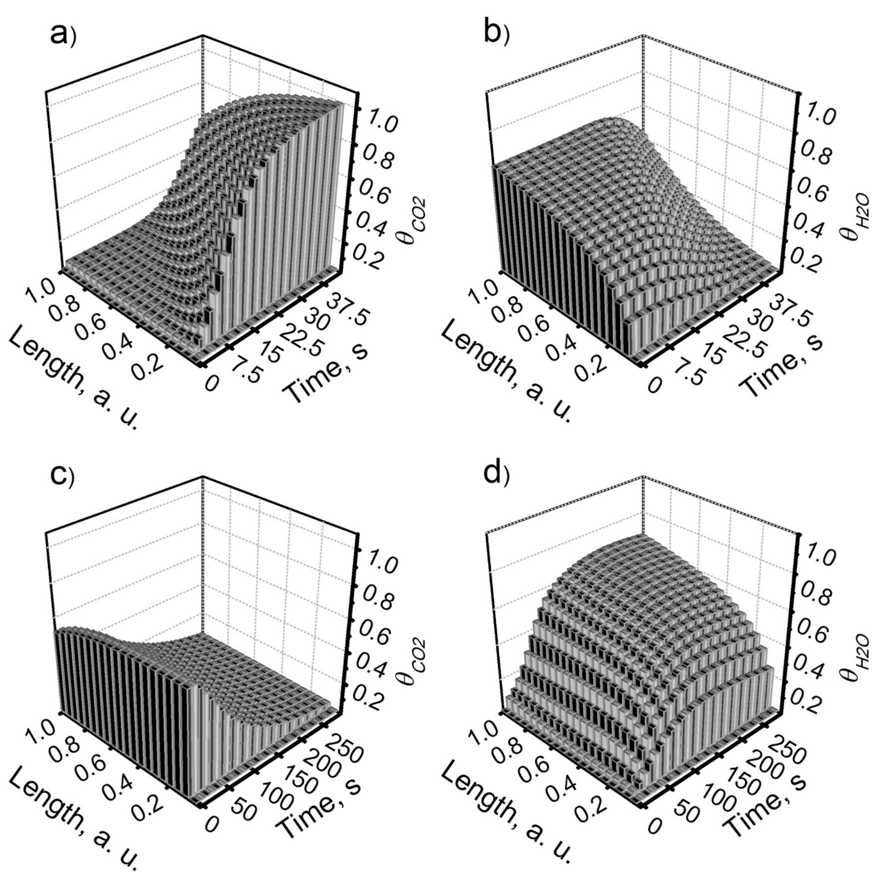

Fig. 3. Longitudinal evolution of the CO_2 and H_2O covering factors during the adsorption (a and b) and the hydrogenation (c and d) for the simulation at 350 °C and the adsorption and hydrogenation period times fixed in 45 and 300 s, respectively.

a value below 1, i.e. θ_{CO2}= 0.6. At this point, it is important to emphasize that the CO_2 adsorption takes place following an adsorption front, which moves forward along the reactor length as the adsorption sites are spent or carbonated. To illustrate the previous statement, Fig. 3a shows the evolution of the CO_2 covering factor (θ_{CO2}) along the reactor length during the adsorption period. As can be observed, at the beginning of the adsorption period, the CO_2 covering factor is 0 along the reactor length, which highlights that the catalyst has been fully regenerated in the previous regeneration period. Then, as the adsorption period proceeds, CO_2 is captured by the catalyst and thus θ_{CO2} increases. Note that the CO_2 is preferentially captured in the reactor entrance, leaving the adsorption sites located downstream empty and available for the CO_2 capture. As the adsorption period continues, the covering factor at the reactor entrance gets more and more saturated, and thus, adsorption sites located downstream start to be filled. At the end of the adsorption period, the CO_2 covering factor at the reactor entrance is 1 (meaning a complete saturation) but the CO_2 covering factor at the reactor outlet is 0.6 (as can be also observed in Fig. 2). Thus, under this operating conditions (t_{CO2}=45 s and t_{H2}=300 s), the catalyst is not fully saturated at the end of the adsorption period.

There is another phenomenon that should be studied during the CO_2 adsorption period, i.e. the release of water displaced by the CO_2 adsorption onto the storage sites to the gas phase. As already reported in the previous section, first CO_2 is adsorbed onto the free adsorption sites (Eq. 10), and once those sites are occupied, the storage of CO_2 proceeds with the displacement of water (Eq. 11). This is the reason why water detection (Fig. 2c) is retarded with respect to the beginning of the adsorption period. Then, water concentration starts to increase but the adsorption period finishes before reaching the maximum value. Again, we will rely on the evolution of the H_2O covering factor along the reactor length during the adsorption period (Fig. 3b) to better understand the state of the catalyst. As can be observed, the H_2O covering factor (θ_{H2O}) is not zero at the beginning of the adsorption period, because some of the adsorption sites are hydrated at the end of the previous hydrogenation period. Note that θ_{H2O} is higher at the reactor outlet due to the dynamics of the regeneration, which will be explained later. As can be observed, θ_{H2O} is hardly affected in the first 15 s of the adsorption, because the adsorption of CO_2 is being taken place in the free adsorption sites. Afterwards, θ_{H2O} starts to decrease at the reactor entrance, where the occupation of the adsorption sites by CO_2 is higher (Fig. 3a). At the end of the adsorption period, water has been completely removed from the adsorption sites (θ_{H2O}=0) at the reactor entrance but there is still water adsorbed at the rear of the reactor. This is because the CO_2 adsorption front does not reach the rear of the reactor and consequently does not displace adsorbed water.

During the hydrogenation period, the evolution of H_2, CH_4 and H_2O is also observed (Fig. 2a). As can be observed, H_2 concentration at the reactor outlet is, at any time, lower than that fed to the reactor (dotted line). This fact indicates that H_2 is being consumed through the Sabatieŕs reaction (Eq. 1) to produce CH_4 and H_2O. CH_4 is immediately detected after the beginning of the hydrogenation period. As the hydrogenation period proceeds, the covering factor of CO_2 is progressively reduced. Eventually θ_{CO2} reaches a value near 0 at the end of the regeneration period, which reveals a complete regeneration of the catalyst. In line with the complete regeneration of the catalyst, CH_4 concentration is insignificant at the effluent of the reactor at the end of the regeneration period. As already explained in the previous section, water detection in the gas phase is retarded with respect to CH_4 because water is adsorbed onto the storage sites. Thus, θ_{H2O} increases with the hydrogenation time. In order to clarify the state of the catalyst during the hydrogenation, we will comment on the evolution of θ_{CO2} and θ_{H2O} along the reactor length during the hydrogenation period (Fig. 3c and d). The first interesting phenomena to highlight is that the regeneration of the catalyst (decrease θ_{CO2}) does not occur following a regeneration front. Opposite to that observed for the CO_2 adsorption in Fig. 3a, the decrease of θ_{CO2} occurs homogeneously along the reactor length. At the end of the regeneration period, the occupation of the adsorption sites by CO_2 is insignificant along the reactor length. With respect to θ_{H2O}, it can be observed that the occupation of the storage sites with H_2O is null in the whole reactor length at the beginning of the hydrogenation period. Afterwards, θ_{H2O} increases due to the adsorption of water (produced through the Sabatier's reaction). Water adsorption explains the retard observed in the detection of water in the gas phase with respect to CH_4 (Fig. 2a). Water preferentially occupies the positions of the rear of the reactor because water produced at the reactor entrance is adsorbed in subsequent positions of the reactor axial coordinate. At the end of the regeneration period, the occupation of the adsorption sites by H_2O is significant, specifically at the rear of the reactor.

To sum up, under this operating conditions (t_{CO2}=45 s and t_{H2}=300 s), the catalyst is not fully saturated with CO_2 at the end of the adsorption period and some water remains adsorbed, specifically in the adsorption sites located at the rear of the reactor. On the other hand, the catalyst is fully regenerated at the end of the hydrogenation period, i.e. almost no CO_2 is adsorbed at any position of the reactor axial coordinate. However, a significant fraction of the storage sites is occupied by H_2O.

3.2.2. Long adsorption period and long hydrogenation period scenario (t_{CO2}/t_{H2}=150/300)

In Fig. 2b we will explain the performance of the catalyst when the adsorption and hydrogenation periods timing is t_{CO2}/t_{H2}= 150/300, representative of long storage and hydrogenation periods. As can be observed, the main difference during the CO_2 adsorption period (with respect to a shorter storage period of 45 s, Fig. 2a) is that the CO_2 concentration at the reactor outlet matches that of the inlet at the end of the adsorption period. This fact reveals a total saturation of the catalyst with CO_2, which can be corroborated by the fact that θ_{CO2} reaches a value of 1. The evolution of the CO_2 covering factor along the reactor length during the adsorption period (Fig. S3a) shows the same trend as in the shorter storage period (Fig. 3a). The unique difference is that a longer storage period of 150 s results in the total saturation of the catalyst with CO_2 in the whole reactor length, as opposite to the partial saturation observed with a shorter duration of 45 s. The second difference is that water concentration peak is totally developed. In fact, at the end of the adsorption period, water concentration is negligible after peaking at 1.1% at 1 min of storage time. Besides, the covering factor of water is also zero. The evolution of the H_2O covering factor along the reactor length during the adsorption period (Fig. S3b) shows that water is totally removed before the adsorption period is finished. No adsorbed water remains at the catalyst surface irrespective the reactor length.

During the hydrogenation period, the performance of the catalyst running with t_{CO2}/t_{H2}= 150/300 s is similar to that shown in Fig. 2a (t_{CO2}/t_{H2}=45/300). The only difference is that with a longer storage time of 150 s the catalyst is fully saturated with CO_2, and thus, during the hydrogenation period CH_4 and H_2O formation is slightly enhanced. Apart from that, the state of the catalyst at the end of the hydrogenation period is almost similar with both timings (t_{CO2}/t_{H2}=45/300 or t_{CO2}/t_{H2}=150/300). A long hydrogenation period of 300 s enables almost a total regeneration of the catalyst, and θ_{CO2} is almost zero irrespective the reactor length (Fig. S3c). As previously explained, the storage sites of the catalyst are partially occupied with H_2O as can be observed in Fig. S3d.

To sum up, under this operating conditions (t_{CO2}=150 s and t_{H2}=300 s), the catalyst is completely saturated with CO_2 at the end of the adsorption period and no water remains adsorbed irrespective the reactor length. On the other hand, the catalyst is fully regenerated at the end of the hydrogenation period. No CO_2 is adsorbed at any position of the reactor axial coordinate but a significant fraction of the storage sites is occupied by H_2O.

3.2.3. Long adsorption period and short hydrogenation period scenario (t_{CO2}/t_{H2}=150/60)

Finally, Fig. 2c shows the performance of the catalyst when the adsorption and hydrogenation periods timing is t_{CO2}/t_{H2}= 150/60, representative of a long storage period and a short hydrogenation period. Due to a shorter regeneration period, the catalyst is not completely regenerated (as will be seen later) and some CO_2 remains adsorbed in the storage sites at the beginning of the adsorption period. In fact, the CO_2 covering factor for the last axial position of the reactor is 0.5 at the beginning of the adsorption period. Consequently, the CO_2 adsorption capacity of the catalyst is limited and the CO_2 breakthrough is earlier detected with respect to the previous t_{CO2}/t_{H2} timings of 45/300 or 150/300. The evolution of the CO_2 covering factor along the reactor length during the adsorption period (Fig. S4a) reveals that θ_{CO2} is around 0.5 irrespective the reactor length. Afterwards, the CO_2 adsorption front evolves (as observed in Figs. 3a and S3a). However, as the CO_2 adsorption period begins with the catalyst partially occupied by CO_2, the saturation is achieved at earlier adsorption times.

Fig. 2c shows that the hydrogenation period finishes before CH_4 concentration peak is totally developed. This information, together with the fact that θ_{CO2} is not cero, points out that only a partial regeneration of the catalyst has been achieved. The evolution of the CO_2 covering factor along the reactor length (Fig. S4c) shows that 60 s of hydrogenation is not enough to complete the regeneration. All the positions of the reactor show a rather homogeneous occupation of CO_2, with a slight tendency to increase θ_{CO2} with the reactor length. This means that the reactor entrance achieves a slightly higher regeneration. Due to the lower regeneration of the catalyst, less H_2O is also produced through the Sabatier's reaction, and thus, less H_2O is adsorbed onto the catalyst (as can be observed in Fig. S4d).

To sum up, under this operating conditions (t_{CO2}=150 s and t_{H2}=60 s), the catalyst is not fully regenerated and some CO_2 together with H_2O remain adsorbed onto the storage sites at the end of the regeneration period. This fact limits the CO_2 adsorption capacity of the subsequent storage period and the CO_2 breakthrough is earlier detected.

3.3. Quantification of catalytic parameters as a function of CO_2 adsorption and hydrogenation periods timing

Once the dynamics of the dual process have been analysed, now the global performance of the catalyst is evaluated based on the following parameters: CO_2 conversion (Eq. 5), H_2 conversion (Eq. 6) and CH_4 production (Eq. 3). First, we will calculate the catalytic parameters for the CO_2 adsorption and hydrogenation timings defined in the previous section. Then, we will extend the analysis for CO_2 adsorption periods ranging from 10 to 150 s and hydrogenation periods ranging from 20 to 300 s. The evolution of CO_2 conversion (X_{CO2}, %), H_2 conversion (X_{H2}, %) and CH_4 production (Y_{CH4}, mmol g^{-1} $cycle^{-1}$) will be shown as a function of the CO_2 adsorption and hydrogenation periods timing in a 3D picture (Fig. 4).

3.3.1. CO_2 conversion

The conversion of CO_2 (Eq. 5) relates the percentage of CO_2 stored onto the catalyst with respect to the amount of CO_2 fed. When the operation is carried out with a CO_2 adsorption and hydrogenation periods timing of 45/300 (Section 3.2.1, Fig. 2a) the CO_2 conversion results in 57%. This high CO_2 conversion is the result of a deep regeneration, which fully regenerates the adsorption sites of the catalyst. This fact enables a high CO_2 adsorption performance at the beginning of the adsorption period. Besides, due to the short CO_2 storage period, the catalyst does not reach saturation and the amount of CO_2 leaving the reactor is limited. The CO_2 conversion is significantly reduced to 12% when the CO_2 adsorption and hydrogenation periods timing is 150/300 (Section 3.2.2, Fig. 2b). The longer duration of the CO_2 storage period, results in the complete saturation of the catalyst. Extending the length of the adsorption period after catalyst saturation penalizes the CO_2 conversion, as no CO_2 is further adsorbed and all the CO_2 fed to the reactor is emitted in the effluent. Finally, the CO_2 conversion is further reduced to 4% when the CO_2 adsorption and hydrogenation periods timing is 150/60 (Section 3.2.3, Fig. 2c). The short regeneration period does not obtain the full regeneration of the catalyst. Consequently, the catalyst is earlier saturated (the CO_2 breakthrough is earlier detected) and the amount of CO_2 emitted in the effluent is enhanced. The result is a further reduction of the CO_2 conversion.

Fig. 4a shows the evolution of the CO_2 conversion (X_{CO2}, %) as a function of the CO_2 adsorption and hydrogenation periods timing. For a given t_{CO2}, the CO_2 conversion increases with t_{H2} due to a deeper regeneration of the catalyst. For a given t_{H2}, the CO_2 conversion decreases with t_{CO2} due to a higher fraction of CO_2 emitted after the saturation of the catalyst. Maximum CO_2 conversion of 95% is obtained with t_{CO2}/t_{H2} of 10/300, i.e. very short adsorption period and long hydrogenation period.

3.3.2. H_2 conversion

The conversion of H_2 is defined by (Eq. 6). When the operation is carried out with a CO_2 adsorption and hydrogenation periods timing of 45/300 (Section 3.2.1, Fig. 2a) the H_2 conversion results in 23%. First, it should be noted that unreacted H_2 is observed at the reactor outlet from the very beginning of the hydrogenation period, which reveals a slow CO_2 desorption and hydrogenation kinetics. In order to fully regenerate the catalyst, long hydrogenation periods are required, as observed in the previous section. However, due to the slow hydrogenation kinetics, high amounts of hydrogen are emitted without being converted, which reduces H_2 conversion. The hydrogen conversion is hardly affected when the CO_2 adsorption time is extended from 45 to 150 s, i.e. t_{CO2}/t_{H2} of 150/300 (Section 3.2.2, Fig. 2b). The only difference among those operating conditions is that a longer adsorption time of 150 s fully saturates the catalyst. Consequently, slightly higher amounts of carbonates are adsorbed on the catalyst surface, which enhances somewhat H_2 conversion to 25%. Finally, hydrogen conversion is significantly promoted to 51% when the operation is carried out with a CO_2 adsorption and hydrogenation periods timing of 150/60 (Section 3.2.3, Fig. 2c).

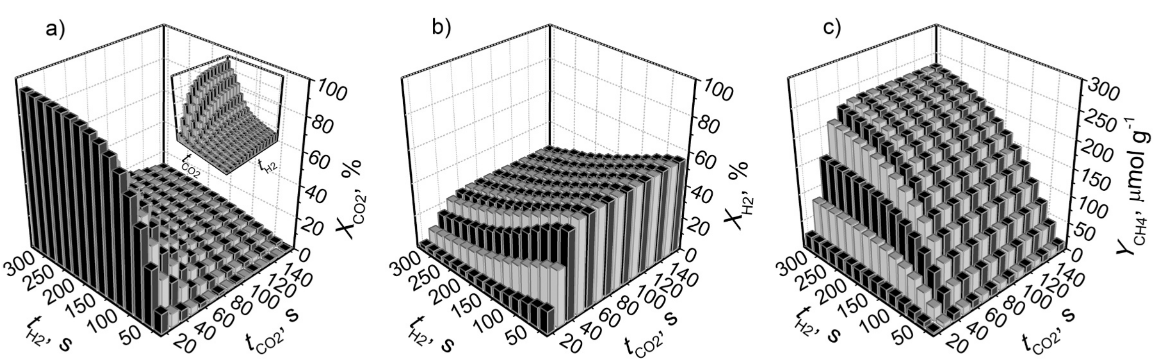

Fig. 4. CH_4 production (Y_{CH4}), CO_2 conversion (X_{CO2}) and H_2 conversion (X_{H2}) with respect to storage and reduction times, in the ranges 10–150 and 20–300 s respectively, at 350 °C and 5.7% of CO_2 and H_2. For a better view, the chart a is included with another orientation.

Due to the short regeneration period of 60 s, the hydrogenation of carbonates occurs with a high local concentration of carbonates, which enhances hydrogenation kinetics, and thus, results in higher H_2 conversion. Note that under these operating conditions, high H_2 conversion is obtained but at the expense of a low CO_2 conversion due to an incomplete regeneration of the catalyst.

Fig. 4b shows the evolution of the H_2 conversion (X_{H2}, %) as a function of the CO_2 adsorption and hydrogenation periods timing. For a given t_{CO2}, the H_2 conversion decreases with t_{H2} due to the progressive inefficient usage of hydrogen, as already explained. For a given t_{H2}, the H_2 conversion is promoted up to t_{CO2}= 60 s, and afterwards, is maintained unaltered. H_2 conversion is promoted in the t_{CO2} range (0–60 s) where a progressive extension of the storage period results in a higher amount of CO_2 stored. Therefore, a higher population of carbonates promotes hydrogen consumption. Storage times longer than 60 s do not change the amount of CO_2 stored (since the catalyst is already fully saturated) and consequently do neither modify H_2 conversion. Maximum H_2 conversion of 56% is obtained for t_{CO2}/t_{H2} of 60/20, i.e. a storage time leading to a complete saturation of the catalyst and a very short hydrogenation period.

3.3.3. CH_4 production

The production of CH_4 is defined by (Eq. 3). When the operation is carried out with a CO_2 adsorption and hydrogenation periods timing of 45/300 (Section 3.2.1, Fig. 2a) the production of CH_4 results in 219 μmol g^{-1}. The long hydrogenation period guarantees the complete regeneration of the catalyst, and thus, CH_4 production is promoted. A slightly higher amount of CH_4 is produced (232 μmol g^{-1}) when the CO_2 adsorption and hydrogenation periods timing is set at 150/300 (Section 3.2.2, Fig. 2b). The extension of the adsorption period leads to the complete saturation of the adsorption sites, and consequently, CH_4 production is slightly enhanced during the hydrogenation period. Finally, CH_4 production is significantly reduced to 73 μmol g^{-1} when the CO_2 adsorption and hydrogenation periods timing is set at 150/60 (Section 3.2.3, Fig. 2c). Due to a short regeneration period, the catalyst is not completely regenerated and CH_4 concentration peak is not totally developed, as observed in Fig. 2c.

Fig. 4c shows the evolution of the CH_4 production (Y_{CH4}, μmol g^{-1}) as a function of the CO_2 adsorption and hydrogenation periods timing. Maximum CH_4 production of 232 μmol g^{-1} is obtained for t_{CO2}/t_{H2} of 60/300, i.e. a storage time leading to a complete saturation of the catalyst and a very long hydrogenation period to promote the complete decomposition of adsorbed carbonates and their hydrogenation to CH_4.

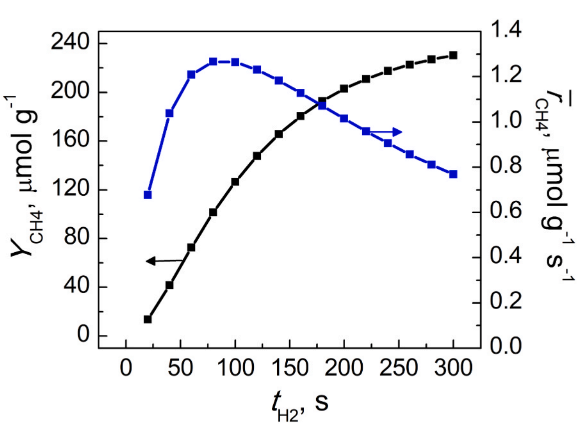

Fig. 5. Evolution of CH_4 production and the average CH_4 formation rate (r_{CH4}) with respect to the hydrogenation time, for a cycle with the adsorption period of 60 s at 350 °C and 5.7% of CO_2 and H_2.

3.4. Optimization and proposed operation strategy

It is obvious that during the CO_2 adsorption and hydrogenation, conversion of CO_2 and H_2 along with CH_4 production should be maximized. However, as already observed in the previous section, it is not possible to look for a unique CO_2 adsorption and hydrogenation period timing (t_{CO2}/t_{H2}) to maximize jointly three catalytic parameters. In principle, results in Fig. 4 suggest adsorption times around 60 s (close to catalyst saturation) and moderate hydrogenation times, which produce a high amount of CH_4 per cycle with a reasonable H_2 conversion. To better select the optimal hydrogenation time, a more appropriate catalytic parameter should be the average formation rate of CH_4 ($\bar{r}_{CH_4}$, μmol g^{-1} s^{-1}). Fig. 5 shows the production of CH_4 and the average formation rate of CH_4, as function of the hydrogenation time. The adsorption time has been set at 60 s in Fig. 5. As explained above (Fig. 4c), the amount of CH_4 produced increases with the hydrogenation time, having a greater slope for low times. On the other hand, the average formation rate has a maximum between 80 and 100 s of hydrogenation. However, 120 s is selected as the optimal hydrogenation time, because also present a high average formation rate of CH_4 and would allow working with three identical beds in parallel, one operating in adsorption and two regenerating producing methane. Thus, under the optimum CO_2 adsorption and hydrogenation periods timing of 60/120 the production of CH_4 results in 148 μmol g^{-1} $cycle^{-1}$ (1.2 μmol g^{-1} s^{-1}) and a CO_2 and H_2 conversion of 25% and 43%, respectively.

This operation strategy, with 3 catalytic reactors, one working in adsorption and the other two regenerating producing SNG, is shown in Fig. 6. In Scheme 1 of Fig. 6, the first reactor operates in adsorption and

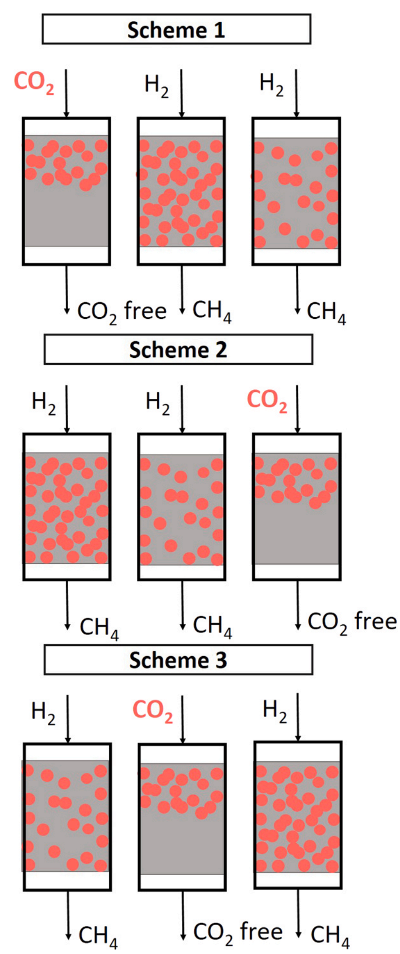

Fig. 6. Proposed arrangement in cycled mode with 3 catalytic beds, one works in adsorption and two in hydrogenation.

the second and third in hydrogenation. However, the reactors that operate in hydrogenation are out of phase. When the hydrogenation begins in the second reactor, it is fully saturated, while the third reactor is partially regenerated, having completed half of the period. In parallel, the first reactor begins the adsorption step fully regenerated. Next, Scheme 2 shows the period change in the first reactor (adsorption to hydrogenation) and in the third reactor (hydrogenation to adsorption), while the second continues to hydrogenation. Subsequently, in Scheme 3, the second reactor changes to adsorption and the third to hydrogenation. Once again, the reactors that work in hydrogenation, both in Schemes 2 and 3, are out of phase. Finally, from Scheme 3 it is changed to Scheme 1 and the operation continues cyclically alternating the schemes.

4. Conclusions

The model used in this work allows predicting the temporal evolution of reagents and products during the dual operation of CO_2 adsorption and methanation, considering that the adsorption sites can be occupied by CO_2, H_2O or simultaneously by both forming a weakly adsorbed bicarbonate. The evaluation of the CO_2 adsorption and hydrogenation yield is carried out in the whole operation, considering the adsorption and hydrogenation performances. As this is a cyclic operation, the state of the catalyst at the beginning of a given period depends on the state of the catalyst at the end of the previous period. In simulations with a short adsorption period and a long hydrogenation period, the catalyst is not fully saturated with CO_2 at the end of the adsorption period and some water remains adsorbed, specifically in the adsorption sites located at the rear of the reactor. On the other hand, the catalyst is fully regenerated at the end of the hydrogenation period and a significant fraction of the storage sites are occupied by H_2O. In simulations with a long adsorption and hydrogenation periods, the catalyst is completely saturated with CO_2 at the end of the adsorption period and no water remains adsorbed. By last, in simulations with a long adsorption period and a short hydrogenation period, the catalyst is not fully regenerated and some CO_2 together with H_2O remain adsorbed onto the storage sites at the end of the regeneration period. This fact limits the CO_2 adsorption capacity of the subsequent storage period.

The global performance of the catalyst is evaluated based on the CO_2 conversion, H_2 conversion and CH_4 production. Maximum CO_2 conversion of 95% is obtained with t_{CO2}/t_{H2} of 10/300, i.e. very short adsorption period and long hydrogenation period. Maximum H_2 conversion of 56% is obtained for t_{CO2}/t_{H2} of 60/20, i.e. a storage time leading to a complete saturation of the catalyst and a very short hydrogenation period. In addition, maximum CH_4 production of 232 μmol g^{-1} is obtained for t_{CO2}/t_{H2} of 60/300, i.e. a storage time leading to a complete saturation of the catalyst and a very long hydrogenation period to promote the complete decomposition of adsorbed carbonates and their hydrogenation to CH_4. Therefore, it is not possible to define a unique CO_2 adsorption and hydrogenation period timing (t_{CO2}/t_{H2}) to maximize all the above catalytic parameters. Adsorption times around 60 s (close to catalyst saturation) and moderate hydrogenation times, which produce a high amount of CH_4 per cycle with a reasonable H_2 conversion, are appropriate. To better select the optimal hydrogenation time, a new catalytic parameter is set, the average formation rate of CH_4 ($\bar{r}_{CH_4}$, μmol g^{-1} s^{-1}). 120 s is selected as the optimal hydrogenation time, which enable to work with three identical beds in parallel, one operating in adsorption and two regenerating producing methane, with a high average formation rate. Thus, under the optimum CO_2 adsorption and hydrogenation periods timing of 60/120 the production of CH_4 results in 148 μmol g^{-1} $cycle^{-1}$ (1.2 μmol CH_4 g^{-1} s^{-1}) and a CO_2 and H_2 conversion of 25% and 43%, respectively.

By last, we are now doing further research to readjust the model to predict the operation in the presence of O_2 and H_2O during the adsorption period and simulate the new optimal operating conditions, on which we will report shortly.

CRediT authorship contribution statement

Alejandro Bermejo-López: Validation, Methodology, Investigation, Writing – original draft. **Beñat Pereda-Ayo:** Conceptualization, Methodology, Visualization, Writing – review & editing. **José A. González-Marcos:** Methodology, Software, Data curation, Supervision, Funding acquisition. **Juan R. González-Velasco:** Conceptualization, Supervision, Project administration, Funding acquisition.

Declaration of Competing Interest

The authors declare that they have no known competing financial interests or personal relationships that could have appeared to influence the work reported in this paper.

Acknowledgements

The financial support from the Economy and Competitiveness Spanish Ministry (CTQ2015-67597-C2-1-R and PID2019-105960RB-C21) and the Basque Government (IT1297-19) is acknowledged. The authors thank for technical and human support provided by SGIker (UPV/EHU Advanced Research Facilities/ ERDF, EU). One of the authors (ABL) also acknowledges the Economy and Competitiveness Spanish Ministry for his PhD grant (BES-2016-077855).

Appendix A. Supporting information

Supplementary data associated with this article can be found in the online version at doi:10.1016/j.cattod.2021.08.023.

References

[1] P. Sabatier, J.B. Senderens, New synthesis of methane, J. Chem. Soc. Faraday Trans. 82 (1902) 333–337.
[2] G. Gahleitner, Hydrogen from renewable electricity: An international review of power-to-gas pilot plants for stationary applications, Int. J. Hydrogen Energy 38 (2013) 2039–2061.
[3] P. Kangas, F. Vidal Vázquez, J. Savolainen, R. Pajarre, P. Koukkari, Thermodynamic modelling of the methanation process with affinity constraints, Fuel 197 (2017) 217–225.
[4] K. Ghaib, F. Ben-Fares, Power-to-Methane: a state-of-the-art review, Renew. Sust. Energy Rev. 81 (2018) 433–446.
[5] Z. Baysal, S. Kureti, CO_2 methanation on Mg-promoted Fe catalysts, Appl. Catal. B 262 (2020), 118300.
[6] G. Garbarino, T. Cavattoni, P. Riani, G. Busca, Support effects in metal catalysis: a study of the behavior of unsupported and silica-supported cobalt catalysts in the hydrogenation of CO_2 at atmospheric pressure, Catal. Today 345 (2019) 213–219.
[7] C. Liang, H. Tian, G. Gao, S. Zhang, Q. Liu, D. Dong, X. Hu, Methanation of CO_2 over alumina supported nickel or cobalt catalysts: effects of the coordination between metal and support on formation of the reaction intermediates, Int. J. Hydrogen Energy 45 (2020) 531–543.
[8] S. Navarro-Jaén, J.C. Navarro, L.F. Bobadilla, M.A. Centeno, O.H. Laguna, J. A. Odriozola, Size-tailored Ru nanoparticles deposited over γ-Al_2O_3 for the CO_2 methanation reaction, Appl. Surf. Sci. 483 (2019) 750–761.
[9] H.T.T. Nguyen, Y. Kumabe, S. Ueda, K. Kan, M. Ohtani, K. Kobiro, Highly durable Ru catalysts supported on CeO_2 nanocomposites for CO_2 methanation, Appl. Catal. A 577 (2019) 35–43.
[10] A.M. Abdel-Mageed, S. Eckle, H.G. Anfang, R.J. Behm, Selective CO methanation in CO_2-rich H_2 atmospheres over a Ru/zeolite catalyst: the influence of catalyst calcination, J. Catal. 298 (2013) 148–160.
[11] S. Chai, Y. Men, J. Wang, S. Liu, Q. Song, W. An, G. Kolb, Boosting CO_2 methanation activity on Ru/TiO_2 catalysts by exposing (001) facets of anatase TiO_2, J. CO2 Util. 33 (2019) 242–252.
[12] O.E. Everett, P.C. Zonetti, O.C. Alves, R.R. de Avillez, L.G. Appel, The role of oxygen vacancies in the CO_2 methanation employing Ni/ZrO2 doped with Ca, Int. J. Hydrogen Energy 45 (2020) 6352–6359.
[13] C. Italiano, J. Llorca, L. Pino, M. Ferraro, V. Antonucci, A. Vita, CO and CO_2 methanation over Ni catalysts supported on CeO_2, Al_2O_3 and Y_2O_3 oxides, Appl. Catal. B 264 (2020), 118494.
[14] A. Quindimil, U. De-La-Torre, B. Pereda-Ayo, J.A. González-Marcos, J.R. González-Velasco, Ni catalysts with La as promoter supported over Y- and BETA- zeolites for CO_2 methanation, Appl. Catal. B 238 (2018) 393–403.
[15] S. Renda, A. Ricca, V. Palma, Precursor salts influence in Ruthenium catalysts for CO_2 hydrogenation to methane, Appl. Energy 279 (2020), 115767.

[16] W. Gac, W. Zawadzki, M. Rotko, M. Greluk, G. Słowik, G. Kolb, Effects of support composition on the performance of nickel catalysts in CO_2 methanation reaction, Catal. Today 357 (2019) 468–482.
[17] M. Thema, F. Bauer, M. Sterner, Power-to-Gas: electrolysis and methanation status review, Renew. Sust. Energy Rev. 112 (2019) 775–787.
[18] A. Porta, C.G. Visconti, L. Castoldi, R. Matarrese, C. Jeong-Potter, R. Farrauto, L. Lietti, Ru-Ba synergistic effect in dual functioning materials for cyclic CO_2 capture and methanation, Appl. Catal. B 283 (2021), 119654.
[19] M.A. Arellano-Treviño, Z. He, M.C. Libby, R.J. Farrauto, Catalysts and adsorbents for CO_2 capture and conversion with dual function materials: limitations of Ni-containing DFMs for flue gas applications, J. CO2 Util. 31 (2019) 143–151.
[20] M.S. Duyar, M.A.A. Treviño, R.J. Farrauto, Dual function materials for CO_2 capture and conversion using renewable H_2, Appl. Catal. B 168–169 (2015) 370–376.
[21] P. Melo Bravo, D.P. Debecker, Combining CO_2 capture and catalytic conversion to methane, Waste Disp. Sust. Energy 1 (2019) 53–65.
[22] I.S. Omodolor, H.O. Otor, J.A. Andonegui, B.J. Allen, A. Alba-Rubio, Dual-function materials for CO_2 capture and conversion: a review, Ind. Eng. Chem. Res. 59 (2020) 17612–17631.
[23] A. Bermejo-López, B. Pereda-Ayo, J.A. González-Marcos, J.R. González-Velasco, Mechanism of the CO_2 storage and in situ hydrogenation to CH_4. Temperature and adsorbent loading effects over Ru-CaO/Al_2O_3 and Ru-Na_2CO_3/Al_2O_3 catalysts, Appl. Catal. B 256 (2019), 117845.
[24] A. Bermejo-López, B. Pereda-Ayo, J.A. González-Marcos, J.R. González-Velasco, Ni loading effects on dual function materials for capture and in-situ conversion of CO_2 to CH_4 using CaO or Na_2CO_3, J. CO2 Util. 34 (2019) 576–587.
[25] A. Bermejo-López, B. Pereda-Ayo, J.A. González-Marcos, J.R. González-Velasco, Alternate cycles of CO_2 storage and in situ hydrogenation to CH_4 on Ni-Na_2CO_3/Al_2O_3: influence of promoter addition and calcination temperature, Sust. Energy Fuels 5 (2021) 1194–1210.
[26] A. Bermejo-López, B. Pereda-Ayo, J.A. González-Marcos, J.R. González-Velasco, Modeling the CO_2 capture and in situ conversion to CH_4 on dual function Ru-Na_2CO_3/Al_2O_3 catalyst, J. CO2 Util. 42 (2020), 101351.
[27] C.J. Keturakis, F. Ni, M. Spicer, M.G. Beaver, H.S. Caram, I.E. Wachs, Monitoring solid oxide CO_2 capture sorbents in action, Chem. Sust. Energy Mater. 7 (2014) 3459–3466.
[28] Q. Zheng, R. Farrauto, A. Chau Nguyen, Adsorption and methanation of flue gas CO_2 with dual functional catalytic materials: a parametric study, Ind. Eng. Chem. Res. 55 (2016) 6768–6776.
[29] L. Falbo, M. Martinelli, C.G. Visconti, L. Lietti, C. Bassano, P. Deiana, Kinetics of CO_2 methanation on a Ru-based catalyst at process conditions relevant for Power-to-Gas applications, Appl. Catal. B 225 (2018) 354–363.